Letters

LLC Resonant Converter With Semiactive Variable-Structure Rectifier (SA-VSR) for Wide Output Voltage Range Application

Hongfei Wu, Yuewei Li, and Yan Xing

***Abstract*—A semiactive variable-structure rectifier (SA-VSR) is proposed for the *LLC* resonant converter to achieve wide output voltage range power conversion. The SA-VSR is composed of two active switches and two diodes. The SA-VSR is operated as a voltage-doubler rectifier when the duty cycle of the active switches is 0.25, whereas it is a voltage-quadrupler rectifier when the duty cycle of the active switches is 0.5. Hence, the output voltage range is extended by adaptively changing the operation mode of the rectifier, which results in reduced switching frequency range, circulating current, and conduction losses of the *LLC* resonant converter. The switches' switching frequency of the SA-VSR is halved in comparison with the switches on the primary side of the *LLC* resonant converter, and zero voltage switching and zero current switching are achieved for all the active switches and diodes, respectively, to reduce the switching losses. The operation principles are analyzed and a 1.5-kW prototype with 400-V input voltage and 100–500-V output voltage is built and tested to verify the feasibility of the proposed method.**

***Index Terms*—*LLC* resonant converter, variable structure, voltage doubler, voltage quadrupler, wide voltage range.**

I. Introduction

LLC resonant converter is gaining much more attention than ever before and has been applied in several applications, such as power supplies for servers [1], front-end converters for renewable power systems [2], and battery chargers for electrical vehicles [3]. Despite its excellent zero-voltage-switching (ZVS) and zero-current-switching (ZCS) performance, an *LLC* resonant converter is still evolving. In fact, many tradeoffs between conversion efficiency and operation range are still necessary to meet the needs of various applications. Hence, new topological variations and innovations have been continuously emerging [4], [5].

High efficiency and high power density can be achieved easily if the *LLC* converter operates around the resonant frequency. However, it is difficult to realize a wide range of voltage/load regulation while maintaining high efficiency within the entire voltage and load ranges. Improved design methods have been proposed to fully utilize the regulation and conversion capabilities of the *LLC* resonant converter, and thus, extend the input and output voltage ranges [6]–[9]. But low efficiency is still inevitable once the switching frequency is far away from the resonant frequency of the resonant tank due to the large circulating current associated with the magnetizing inductance. Improved topologies with variable-structure principles have been proposed for the *LLC* resonant converter to extend the voltage gain range. In [10], a hybrid three-level configuration is proposed for the *LLC* resonant converter, where the voltage gain range is doubled using three-level and two-level operation modes. In [11], a hybrid full-bridge and half-bridge operation scheme is proposed for wide input voltage application. In this case, the voltage gain range of the *LLC* converter is doubled as well. In [12], a two-transformer-based *LLC* resonant converter is proposed to extend the voltage gain range by adaptively changing the equivalent turns ratio and magnetizing inductance of the resonant converter. The voltage gain range can be extended and the switching frequency range of the *LLC* resonant converter can be reduced by using these methods. However, these primary-side variable-structure topologies are suitable for wide input voltage range with constant output voltage applications, but unsuitable for the wide output voltage range with constant input voltage applications, e.g., the battery charger for electric vehicles. When the output voltage increases, even though the primary-side structure is changed, the flux and the magnetizing current at secondary-side winding of the transformer will increase, resulting in higher core and conduction losses.

To overcome the drawbacks of the *LLC* converter, achieving wide output voltage range and meantime maintaining high conversion efficiency, this letter proposed a novel semiactive variable-structure rectifier (SA-VSR) for the *LLC* converter. The output voltage range is doubled by adaptively operating the SA-VSR as a voltage-doubler and a voltage-quadrupler rectifier (VQR).

II. Proposed *LLC* Resonant Converter With SA-VSR and Operation Principles

A. Proposed Topology

A full-bridge *LLC* resonant converter with the proposed SA-VSR is shown in Fig. 1. The SA-VSR is composed of a switched

Manuscript received October 3, 2015; revised October 28, 2015; accepted November 5, 2015. Date of publication November 10, 2015; date of current version December 10, 2015. This work was supported in part by the National Natural Science Foundation of China under Grant 51407092, in part by the Natural Science Foundation of Jiangsu Province, China, under Grant BK20140812, and in part by the Jiangsu Province University Outstanding Science and Technology Innovation Team Project.

The authors are with the Jiangsu Key Laboratory of New Energy Generation and Power Conversion, College of Automation Engineering, Nanjing University of Aeronautics and Astronautics, Nanjing 210016, China (e-mail: wuhongfei@nuaa.edu.cn; lyw0723@nuaa.edu.cn; xingyan@nuaa.edu.cn).

Color versions of one or more of the figures in this paper are available online at http://ieeexplore.ieee.org.

Digital Object Identifier 10.1109/TPEL.2015.2499306

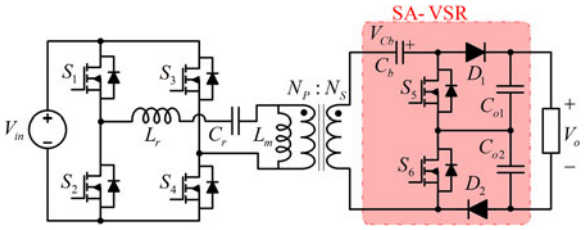

Fig. 1. Topology of the proposed *LLC* resonant converter with SA-VSR.

capacitor C_b, two active switches S_5 and S_6, two diodes D_1 and D_2, and two output capacitors C_{o1} and C_{o2}. With the help of the two active switches S_5 and S_6, the discharging circuit of the switched capacitor C_b can be regulated and changed. If the discharging current of C_b is always supplied to the series combination of C_{o1} and C_{o2}, the SA-VSR is operated as a voltage-doubler rectifier (VDR), in which case the output voltage V_o is two times of the voltage on C_b, V_{Cb}, i.e., $V_o = 2V_{Cb}$. If the discharging current of C_b is supplied to C_{o1} and C_{o2} alternatively, the SA-VSR is operated as a voltage-quadrupler rectifier, in which case $V_o = 4V_{Cb}$. Meanwhile, the switches and diodes in the SA-VSR only sustain half of the output voltage due to the symmetrical configuration of the rectifier.

B. Operation Principles

The operation principles of the primary-side switches $S_1 - S_4$ are the same as the conventional full-bridge *LLC* resonant converter. All the switches $S_1 - S_4$ have the constant duty cycle of 0.5, S_1 and S_4 turn ON and OFF simultaneously, while S_2 and S_3 share the same gate signal. Variable frequency modulation is adopted to regulate the output voltage and power. The switching frequency f_S can be less, equal or greater than the resonant frequency f_r of the resonant tank. Considering the ZVS and ZCS performance, $f_S \leq f_r$ is preferred. The secondary-side switches S_5 and S_6 are driven in the interleaved fashion (with 180° phase shift). Meanwhile, only one of the two switches S_5 and S_6 is turned ON when the primary-side switches S_2 and S_3 are turned ON. Therefore, the switching frequency of S_5 and S_6 is halved in comparison with the switching frequency of the switches S_2 and S_3. When the converter operates in the VDR mode, the duty cycle of S_5 and S_6 $d_{S56} = 0.25$, whereas $d_{S56} = 0.5$ if the converter operates in the VQR mode. The operation principles with different frequency is similar with each other, only the case $f_S < f_r$ is analyzed here.

1) VDR Mode: The key waveforms of the proposed *LLC* converter in the VDR mode is shown in Fig. 2. There are six switching stages in one switching cycle. The equivalent circuit of each switching Stage is shown in Fig. 3.

Stage I [t_0, t_1][See Fig. 3(a)]: Before t_0, S_1 and S_4 are ON, all the switches and diodes on the secondary side are OFF, L_r and L_m resonates with C_r. At t_0, S_1 and S_4 are OFF, the body diodes of S_2 and S_3 are ON due to the positive resonant current. Meanwhile, the body diodes of S_5 and S_6 are ON.

Stage II [t_1, t_2][See Fig. 3(b)]: At t_1, S_2, S_3, and S_5 are turned ON with ZVS.

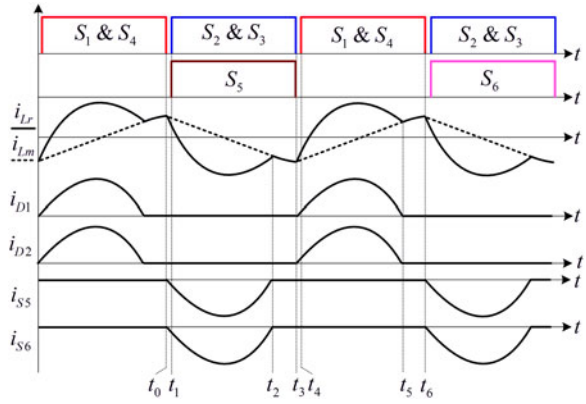

Fig. 2. Key waveforms of the converter in the VDR mode.

During Stages I and II, L_r resonates with C_r, and the capacitor C_b is charged by the resonant current. The voltage $v_{\rm NS}$ applied on the secondary winding of the transformer is

$$v_{\rm NS} = -V_{\rm Cb}. \tag{1}$$

Stage III [t_2, t_3][See Fig. 3(c)]: At t_2, the body diode of S_6 is OFF. L_r and L_m begins to resonates with C_r.

Stage IV [t_3, t_4][See Fig. 3(d)]: At t_3, S_2, S_3, and S_5 are turned OFF. It should be noted that S_5 is turned OFF with zero voltage and zero current. The body diodes of S_1 and S_4 are ON. Meanwhile, the rectifying diodes D_1 and D_2 are ON.

Stage V [t_4, t_5][See Fig. 3(e)]: At t_4, S_1 and S_4 are turned ON with ZVS.

During Stages IV and V, L_r resonates with C_r, and the capacitor C_b is discharged by the resonant current. The discharging current is supplied to C_{o1} and C_{o2} simultaneously because both S_5 and S_6 are OFF. Therefore, the voltage applied on the secondary winding of the transformer is

$$v_{\rm NS} = V_o - V_{\rm Cb}. \tag{2}$$

Stage VI [t_5, t_6][See Fig. 3(f)]: At t_5, the discharging current decreases to zero, and the diodes D_1 and D_2 are OFF. L_r and L_m begins to resonate with C_r.

It should be noted that the switch S_5 is operated as a synchronous rectifying switch and S_6 is OFF in this switching cycle. In the next switching cycle, the roles of S_5 and S_6 will be exchanged. The operation principles are similar and not analyzed again.

2) VQR Mode: The key waveforms of the converter in the VQR mode are shown in Fig. 4. In comparison with the VDR mode, the only difference is that the duty cycle d_{S56} of the secondary-side switches S_5 and S_6 is increased to 0.5. So, S_5 and S_6 are driven complementary, but the switching frequency of S_5 and S_6 is halved as well compared to the primary-side switches. There are six switching stages in one switching period.

The operation principles and equivalent circuits of the Stages I [t_0, t_1], II [t_1, t_2], and III [t_2, t_3] in the VQR mode are the same as that of Stages I, II, and III, respectively, in the VDR mode.

Stage IV [t_3, t_4]: At t_3, S_2 and S_3 are turned OFF, but S_5 stays in ON-state. The body diodes of S_1 and S_4 are ON, and the rectifying diode D_2 is ON, as shown in Fig. 5(a).

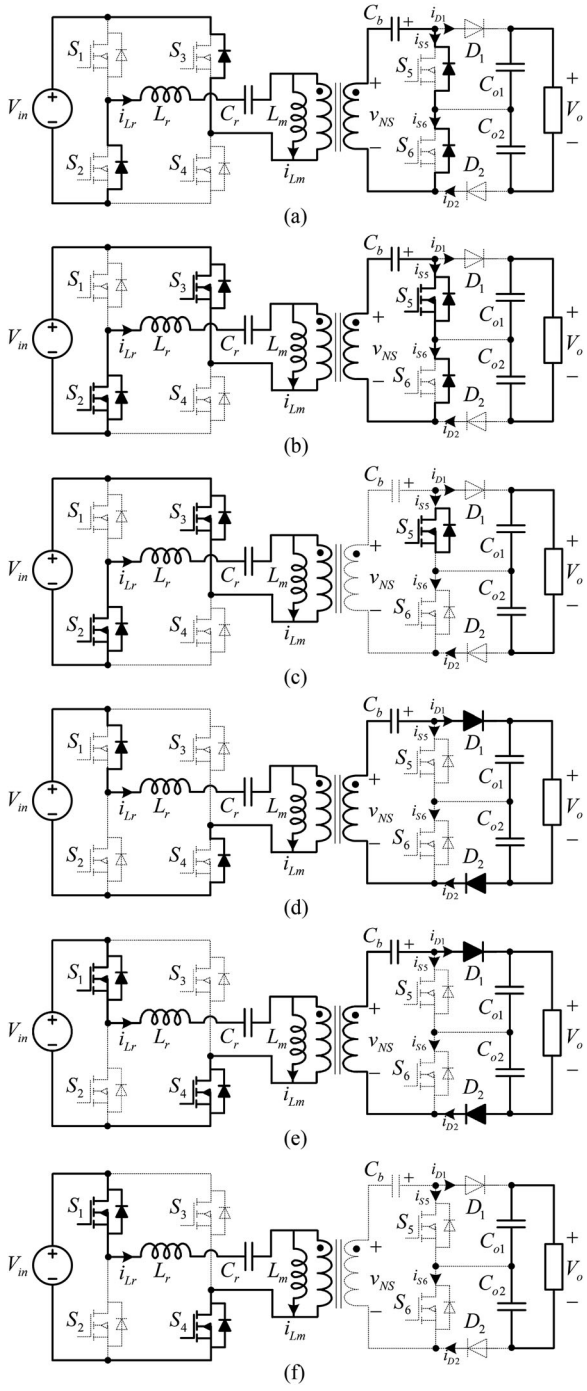

Fig. 3. Equivalent circuit of the VDR mode, (a) [t_0, t_1], (b) [t_1, t_2], (c) [t_2, t_3], (d) [t_3, t_4], (e) [t_4, t_5], and (f) [t_5, t_6].

Stage V [t_4, t_5]: At t_4, S_1 and S_4 are turned ON with ZVS.

During stages IV and V, L_r resonates with C_r and C_b is discharged. Since S_5 is ON, the discharging current of C_b is supplied to the output capacitor C_{o2} only. Therefore, the voltage applied on the secondary winding of the transformer is

$$v_{\mathrm{NS}} = \frac{V_o}{2} - V_{\mathrm{Cb}}. \tag{3}$$

It should be noted that, in the next switching cycle, the discharging current will be supplied to C_{o1} only because S_6 is ON and S_5 is OFF in the next switching cycle. As a results, the voltages on C_{o1} and C_{o2} are autobalanced and equal to 0.5 Vo.

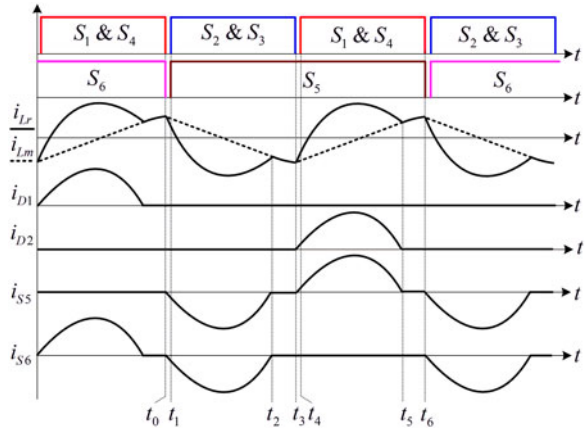

Fig. 4. Key waveforms of the converter in the VQR mode.

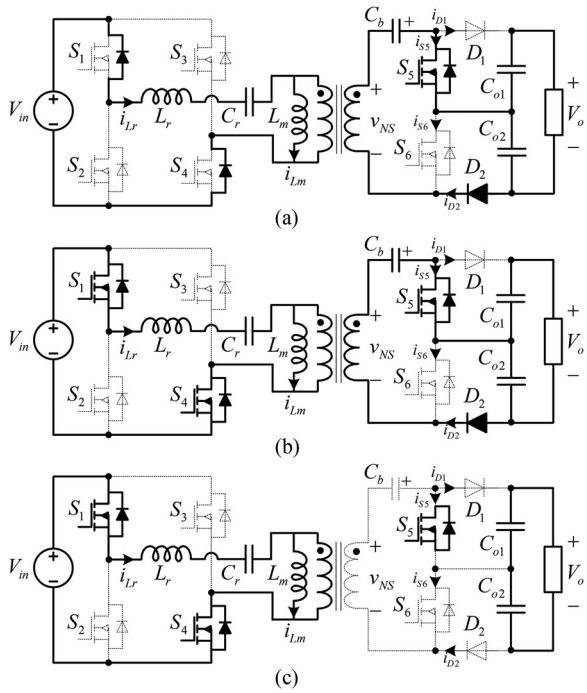

Fig. 5. Equivalent circuit of the VQR mode, (a) [t_3, t_4], (b) [t_4, t_5], and (c) [t_5, t_6].

Stage VI [t_5, t_6]: At t_5, the current flowing through D_2 decreases to zero and D_2 is OFF naturally with zero current. There is no current supplied to the output in this stage even though S_5 is ON. On the primary side, L_r and L_m begins to resonates with C_{r}.

III. Characteristics and Analysis

A. Voltage Gain

When the converter operates in the VDR mode, according to (1), (2), and the volt-second balance of the transformer

$$-V_{\mathrm{Cb}} + (V_o - V_{\mathrm{Cb}}) = 0. \tag{4}$$

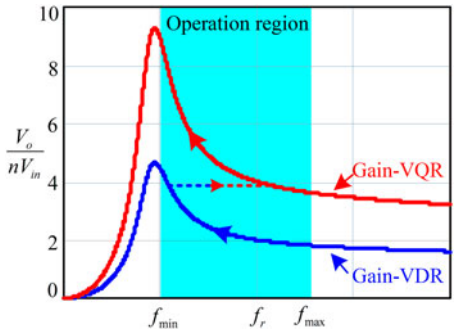

Fig. 6. Gain curves of the proposed converter.

Therefore

$$V_o = 2V_{\mathrm{Cb}}. \tag{5}$$

Similarly, when the converter operates in the VQR mode, according to (1) and (3)

$$V_o = 4V_{\mathrm{Cb}}. \tag{6}$$

When the power is transferred to the secondary side, the voltage applied on the secondary winding of the transformer, is always V_{Cb}, hence, the normalized voltage gain of the resonant tank, M_R, is defined to be

$$M_R = \frac{N_P V_{\mathrm{Cb}}}{N_S V_{\mathrm{in}}} = \frac{V_{\mathrm{Cb}}}{nV_{\mathrm{in}}} \tag{7}$$

where N_P, N_S, and n are the primary winding, secondary winding, and turns ratio of the transformer. Then, the normalized voltage gain of the proposed *LLC* resonant converter, M_{LLC}, can be derived as

$$M_{\mathrm{LLC}} = \frac{V_o}{nV_{\mathrm{in}}} = \begin{cases} 2M_R, \text{VDR mode} \\ 4M_R, \text{VQR mode.} \end{cases} \tag{8}$$

The normalized gain curves of the proposed converter is illustrated in Fig. 6, where it is shown that the gain range can be extended by adaptively change the operation mode of the SA-VSR. An extremely wide output voltage range can be achieved with a narrow switching frequency of the resonant tank. In practice, in order to regulate the output voltage continuously, the maximum voltage gain of the VDR mode must be no less than the minimum voltage gain of the VQR mode.

B. Feedback Control and Mode Transition

The control block diagram of the proposed converter is shown in Fig. 7. The output power is regulated with closed-loop control by varying the switching frequency of the switches, while the operation mode and structure of the SA-VSR is determined by the duty cycle of the switches S_5 and S_6. As shown in Fig. 7, the operation mode of the SA-VSR is open-loop controlled and selected by comparing the output voltage v_o and the threshold voltage V_{th}. In the VDR mode, the duty cycle of S_5 and S_6 is $d_{S56} = 0.25$, whereas $d_{S56} = 0.5$ in the VQR mode.

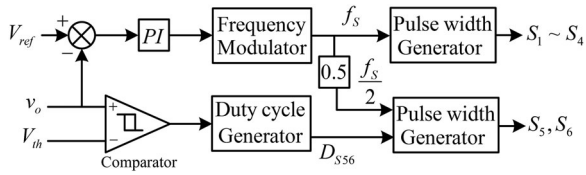

Fig. 7. Control block diagram of the proposed converter.

When $0.25 < d_{S56} < 0.5$, the converter will operates in a hybrid mode, which is a combination of the VDR and VQR modes. As the duty cycle d_{S56} increases, the average operation time of the VDR mode will decrease and the average operation time of the VQR mode will increase, which means the normalized voltage gain will increase and be proportional to d_{S56}. Therefore, to switch the operation mode of the converter from the VDR mode to the VQR mode smoothly, we only need to increase d_{S56} from 0.25 to 0.5 continuously. During the mode transition, the output voltage/power can be regulated as well by varying the switching frequency of switches with closed-loop control. Therefore, the mode transition can be realized very easily.

C. Soft-Switching Performance

ZVS can be achieved for the primary-side active switches within in the entire operation range with the proposed converter, which is the same as the conventional *LLC* resonant converter. Meanwhile, according to the operation principles of the converter, ZVS turn ON and ZCS turn OFF can be realized for all the secondary-side active switches and diodes, respectively. Furthermore, when the capacitor C_b is charged, one of the two switches S_5 and S_6 is operated as a synchronous rectifying switch, which means the charging current only flows through one body diode of the two active switches on secondary side.

D. Performance Comparison

The proposed *LLC* resonant converter is more suitable for wide output voltage range applications, while the primary-side variable-structure *LLC* resonant converters presented in [10]–[12] are good candidates for wide input voltage range applications. Among these solutions, the converters presented in [10] and [11] are more cost effective, because there is no additional component introduced in comparison with the conventional *LLC* resonant converter. However, two active switches have to be used on the secondary side of the proposed converter, which will lead to higher cost and complicate the driving and control circuit. Meanwhile, the current on the secondary side of the proposed converter always flows through two devices that may lead to high conduction loss. However, the voltage stress of the secondary-side switches/diodes is only half of the output voltage. Therefore, the proposed converter is more suitable for high output voltage applications. It is clear that each solution has its advantages and disadvantages. It should be noted that the proposed SA-VSR and the primary-side variable-structure solutions can be combined to further extend the operation voltage ranges of the conventional *LLC* resonant converter.

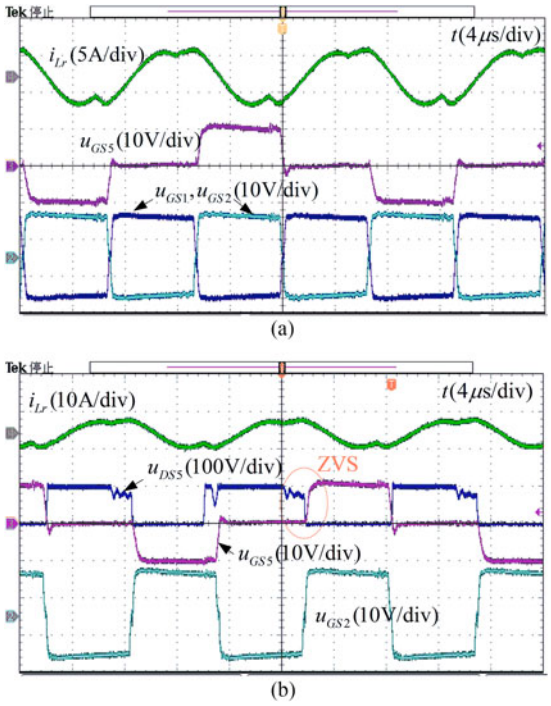

Fig. 8. Switching waveforms in the VDR mode, (a) $i_{Lr}, u_{\mathrm{GS5}}, u_{\mathrm{GS1}}$ and u_{GS2}, (b) $i_{Lr}, u_{\mathrm{GS5}}, u_{\mathrm{DS5}}$ (drain–source voltage of S_5), and u_{GS2}.

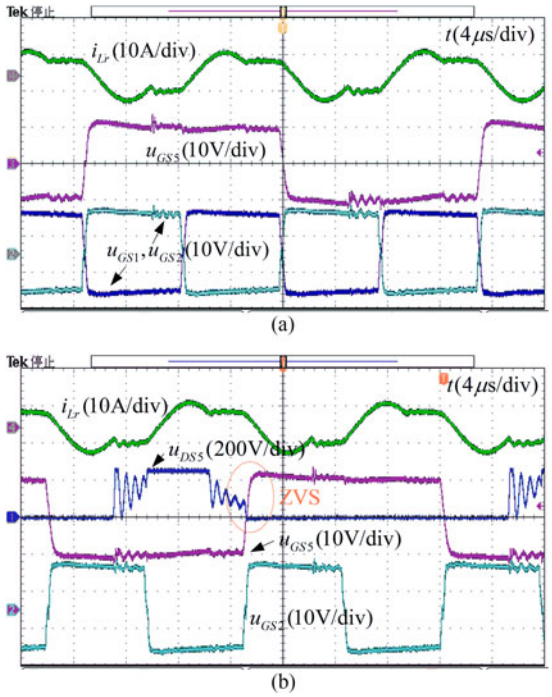

Fig. 9. Switching waveforms in the VQR mode, (a) $i_{Lr}, u_{\mathrm{GS5}}, u_{\mathrm{GS1}}$ and u_{GS2}, (b) $i_{Lr}, u_{\mathrm{GS5}}, u_{\mathrm{DS5}}$ (drain-source voltage of S_5), and u_{GS2}.

IV. Experimental Results

A 1.5-kW experimental prototype for battery charging application is built based on the proposed *LLC* resonant converter. The parameters are as follows. $V_{\mathrm{in}} = 400$ V $\pm$ 10V, $V_o = 100$–500 V, maximum output current $I_{o\max} = 3$A, S_1–S_4: IXTH28N50Q, S_5 and S_6: IRFP4868, D_1 and D_2: DPG30C400HB, transformer's turns ratio $n = N_P : N_S = 32 : 6$, $L_m = 400$ μH, $L_r = 130$ μH, $C_r = 20$ nF, the resonant frequency $f_r = 100$ kHz, and the switching frequency range is about 70–150kHz. The control shown in Fig. 7 is adopted and realized using a digital signal processor (DSP) MC56F8247. According to these parameters, the output voltage of the resonant converter at the resonant frequency is 150 and 300 V in the VDR mode and VQR mode, respectively.

The steady-state switching waveforms of the proposed *LLC* converter in the VDR mode with output current $I_o = 3$A and output voltage $V_o = 200$ V are shown Fig. 8. It can be seen that the waveforms are the similar to the conventional *LLC* converter. The ON-time of S_5 is the same as that of S_2, but the duty cycle of S_5 is 0.25 while the duty cycle of S_2 is 0.5, which means the switching frequency of S_5 is halved in comparison with S_2. From Fig. 8(b), it can be seen that ZVS is achieved for the secondary-side switch S_5. Meanwhile, the maximum drain–source voltage of S_5 is only 100 V, which is a half of the output voltage.

The steady-state switching waveforms of the proposed *LLC* converter in the VQR mode with output current $I_o = 3$A and output voltage $V_o = 500$ V are shown in Fig. 9. It can be seen that, in the VQR mode, the ON-time of S_5 is two times of that of S_1 and S_2, and the duty cycle of S_5 is 0. 5. From Fig. 9(b), it can be seen that ZVS is achieved as well for the secondary-side switch S_5. S_5 only sustain 250-V voltage stress when the output voltage is 500 V. The steady-state waveforms satisfy the analysis pretty well.

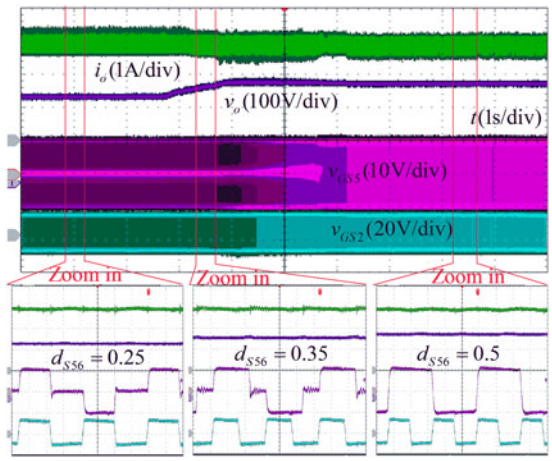

Fig. 10. Experimental waveforms of mode transition.

The mode transition waveforms are shown in Fig. 10. This converter is designed for an electric vehicle battery charger application. Resistive load is used to test the mode transition waveforms. The threshold voltage is set at 285 V. When the output voltage is lower than 285 V, the converter operates in the VDR mode, whereas it works in the VQR mode when the output voltage is higher than 285 V. The mode transition is triggered by changing the load resistance and increasing the output voltage.

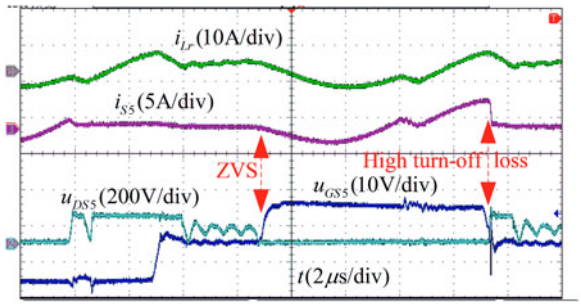

Fig. 11. ZVS waveforms of S_5 when $d_{S56} = 0.35$.

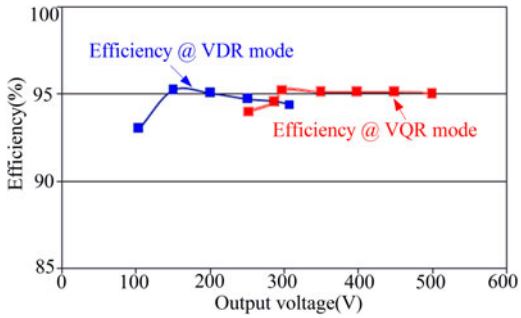

Fig. 12. Efficiency versus output voltage with $I_o = 3$A.

It can be seen that smooth mode transition is achieved and the output current is controlled to be 3 A when the output voltage increases.

In steady state, the ZVS performance of the proposed converter is exactly the same as the conventional *LLC* resonant converter, which means ZVS can be achieved within the entire voltage and load ranges. However, it should be noted that ZVS can be achieved as well even when the converter operation in the transition mode with $0.25 < d_{S56} < 0.5$. The switching waveforms of S_5 when $d_{S56} = 0.35$ are shown in Fig. 11. It can be seen that zero-voltage turn ON has been realized. However, zero-current turn OFF cannot be achieved, and the turn OFF loss is high due to the high turn OFF current. Therefore, $0.25 < d_{S56} < 0.5$ is not recommended for steady-state operation.

The efficiency of the proposed *LLC* resonant converter is tested and shown in Fig. 12. It can be seen that higher efficiency can be achieved with the VDR mode when the output voltage is lower than 285 V, while higher efficiency is achieved with the VQR mode when the output voltage is higher than 285 V, which means 285 V is preferred for the threshold voltage. Experimental results indicate that high efficiency within the entire output voltage range (100–500 V) can be achieved by dynamically changing the operation mode and structure of the rectifier.

V. Conclusion

A straightforward and simple method for extending the output voltage range of the *LLC* resonant converter has been proposed and verified in this letter. In order to increase the output voltage range while reduce the normalized voltage gain range of the *LLC* resonant converter, an SA-VSR has been proposed. The SA-VSR can works as either a VDR or a VQR. Therefore, in comparison with the conventional *LLC* resonant converter with a passive rectifier, the output voltage range of the proposed converter can be doubled. Duty-cycle control is applied to the SA-VSR to adaptively change the operation mode and achieve smooth mode transition. ZVS turn ON and ZCS turn OFF have been achieved for all of the active switches and diodes, respectively, in the converter. The switches and diodes in the SA-VSR only suffer from half of the output voltage, which makes the proposed rectifier suitable for high-voltage applications. Experimental results on a 1.5-kW prototype with 400-V input voltage and 100–500V output voltage verify the effectiveness and feasibility of the proposed solution.

References

[1] H. Nguyen, R. Zane, and D. Maksimovic, "ON/OFF control of a modular DC-DC converter based on active-clamp LLC modules," *IEEE Trans. Power Electron*, vol. 30, no. 7, pp. 3748–3760, Jul. 2015.

[2] Q. Zhang, C. Hu, L. Chen, A. Amirahmadi, N. Kutkut, Z. J. Shen, and I. Batarseh, "A center point iteration MPPT method with application on the frequency-modulated LLC mocroinverter," *IEEE Trans. Power Electron.*, vol. 29, no. 3, pp. 1262–1274, Mar. 2014.

[3] H. Haga and F. Kurokawa, "A novel modulation method of the full bridge three-level LLC resonant converter for battery charger of electrical vehicles," *IEEE Energy Convers. Congr. Expo.*, 2015, pp. 5498–5504.

[4] X. Sun, Y. Shen, Y. Zhu, and X. Guo, "Interleaved boost-integrated LLC resonant converter with fixed-frequency PWM control for renewable energy generation applications," *IEEE Trans. Power Electron.*, vol. 30, no. 8, pp. 4312–4326, Aug. 2015.

[5] H. Wu, T. Mu, X. Gao, and Y. Xing, "A secondary-side phase-shift-controlled LLC resonant converter with reduced conduction loss at normal operation for hold-up time compensation application," *IEEE Trans. Power Electron.*, vol. 30, no. 5, pp. 5352–5357, Oct. 2015.

[6] Z. Fang, T. Cai, S. Duan, and C. Chen, "Optimal design methodology for LLC resonant converter in battery charging applications based on time-weighted average efficiency," *IEEE Trans. Power Electron.*, vol. 30, no. 10, pp. 5469–5483, Oct. 2015.

[7] C. Buccella, C. Cecati, H. Latafat, P. Pepe, and K. Razi, "Observer-based control of LLC DC/DC resonant converter using extended describing functions," *IEEE Trans. Power Electron.*, vol. 30, no. 10, pp. 5881–5891, Oct. 2015.

[8] R. Beiranvand, B. Rashidian, M. R. Zolghadri, and S. M. H. Alavi, "A design procedure for optimizing the LLC resonant converter as a wide output range voltage source," *IEEE Tran. Power Electron.*, vol. 27, no. 8, pp. 3749–3763, Aug. 2012.

[9] F. Musavi, M. Craciun, D. S. Gautam, W. Eberle, and W. G. Dunford, "An LLC resonant DC-DC converter for wide output voltage range battery charging applications," *IEEE Trans. Power Electron.*, vol. 28, no. 12, pp. 5437–5445, Dec. 2013.

[10] K. Jin and X. Ruan, "Hybrid full-bridge three-level LLC resonant converter—A novel DC-DC converter suitable for fuel-cell power system," *IEEE Trans. Ind. Electron.*, vol. 53, no. 5, pp. 1492–1503, Oct. 2006.

[11] Z. Liang, R. Guo, G. Wang, and A. Huang, "A new wide input range high efficiency photovoltaic inverter," in *Proc. IEEE Energy Convers. Congr. Expo.*, 2010, pp. 2937–2943.

[12] H. Hu, X. Fang, F. Chen, Z. J. Shen, and I. Batarseh, "A modified high-efficiency LLC converter with two transformers for wide input-voltage range applications," *IEEE Trans. Power Electron.*, vol. 28, no. 4, pp. 1946–1960, Apr. 2013.